Continuous one-dimensional elastic macro-elements as a natural alternative crack detection tool to the spectral finite element method

T. SZOLC

Institute of Fundamental Technological Research PAN
ul. Świętokrzyska 21, 00-049 Warsaw, Poland

IN THE PAPER the wave method of fault identification in rods, shafts and beams is proposed. This method is based on dynamical models consisting of structural macro-elements with continuously distributed inertial-visco-elastic properties, represented by individual segments of the investigated objects. The fault detection and identification reduces to simulations of diagnostic wave propagation and wave reflections in these models. These simulations are performed directly in time domain by means of analytical solutions of the partial differential equations of motion. In the computational examples, reflected waves were sought in the cracked cantilever rod and beam. These results have been compared with the analogous findings obtained by other authors, using the spectral finite element method. The natural continuous character of the applied elastic macro-elements enables us to apply a straightforward simulation of wave effects, which makes the proposed approach a promising and effective tool for fault identification in various structures and mechanical systems.

1. Introduction

CURRENTLY, an intensive development of theoretical and experimental methods of detection and localization of cracks and other imperfections in responsible parts of machines and structures is can be observed. The methods based on diagnostic wave propagation in the tested element seem now to be particularly advantageous for this purpose, because they are much more sensitive to small imperfections than the typical vibratory fault detection methods, commonly applied to the rotor machines, for example. The wave methods are reduced to investigations of elastic wave propagation and reflections in the considered parts of machines and structures, regarded as one- or two-dimensional homogeneous continuous media, such as rods, shafts, beams and plates. For this purpose, the spectral finite element method (SFEM) is one of the most convenient and powerful computational tools, which has been developed in recent years and described in numerous publications, e.g. [1–9] written by authors working in the famous world-wide research centres in the field of machine and structure dynamics.

In the presented paper, an alternative method of crack detection in responsible parts of mechanical systems and structures is proposed. This approach is also based on the wave propagation analysis in the above-mentioned continuous media. In this method, the tested elastic rods, shafts and beams are regarded as finite structural elements, but without any discretization of their inertial-visco-elastic properties. Because these properties are continuously distributed along the spatial co-ordinates, contrary to the classical finite elements and similarly to [10], these structural elements proposed here are called visco-elastic continuous macro-elements (V-ECM). The visco-elastic continuous macro-elements have been applied so far in the discrete-continuous models of mechanical systems used in the advanced vibration analyses of drive systems in [10, 11], rotor machines in [10, 12, 13], structures under moving loads in [10] and in vibration analyses of the railway vehicle running gears in [10, 14–16]. The V-ECM have been also used for fatigue life prediction of cracked rotor-shafts of the rotating machines in [17]. In the presented paper, the visco-elastic continuous macro-elements are applied for crack detection in the elastic rod and beam using the wave propagation approach. The proposed method has been additionally improved by an introduction of the continuous "throw-off" macroelement, which conducts the unnecessary reflected waves out of the investigated system. The proper mathematical formulation of the problem for the visco-elastic continuous macro-elements, together with the corresponding computational results, are compared respectively with the mathematical description and the numerical results obtained for the same objects by means of the spectral finite element method.

2. Characterization of the spectral finite element method (SFEM)

The classical finite element method (FEM) is an approximate numerical approach based on the local formulation of the Rayleigh–Ritz method, [18]. In the typical finite elements the shape functions belong to the class of admissible functions satisfying only geometrical conformity conditions in the nodes. In order to study the high-frequency vibratory, impact or wave processes, the classical finite element formulation requires a very high discretization mesh densities, which usually leads to detrimental computational consequences. According to the above, despite a very high applicability and reliability of the finite element method, the spectral finite element method (SFEM) has been developed as an alternative tool, in which the drawbacks of the FEM mentioned above are avoided and the obvious advantages are still taken into consideration.

As it follows from [1–9], in the spectral finite element method, as the shape functions the eigenfunctions are used, which satisfy geometrical and dynamic boundary conditions in the element nodal cross-sections, as well as the par-

tial differential motion equation describing the character of deformation of the considered spectral finite element, e.g. rod-, beam- or plate-element. The eigenfunctions are obtained by means of analytical solving of the motion equation using the wave solution

$$(2.1) \qquad u(x,t) = e^{-j(kx-\omega t)},$$

where $u(x,t)$ denotes the unknown displacement expressed as a function of the spatial co-ordinate x and time t, $k = {}^{\omega}\!/_{\nu}$ is the wave number, ω denotes the angular frequency of the wave propagating with velocity v and j is the imaginary number. It is easy to remark that solution (2.1) can be also reduced to the form of a solution by separation of variables, which leads to identical characteristic equations for wave numbers as in the case of typical vibration problems of continuous systems described e.g. in [18]. Nevertheless, these eigenfunctions do not correspond to the natural frequencies of the investigated mechanical system or structure but to a current frequency of the vibrating spectral finite element. In order to perform a high-frequency analysis using the spectral finite element method, contrary to the classical finite element formulation, a given spectral finite element can be arbitrarily long and no additional discretization of its inertial-visco-elastic properties by an increase of mesh density is required.

From the viewpoint of comparison of the mathematical formulation for the spectral finite element method (SFEM) with the mathematical formulation for the approach based on the visco-elastic continuous macro-elements (V-ECM), which is going to be presented below, we should remind that the eigenfunctions of the spectral finite elements have the form of sums of exponential functions of the spatial co-ordinate x and the roots of the characteristic equation k_n, [1–9],

$$(2.2) \qquad \hat{u}(x) = \sum_{m=1}^{M} \sum_{n=1}^{N} A_{nm} e^{-k_n(x-L)},$$

where M denotes the number of samples applied and L is the geometric dimension of the spectral finite element. Number of these roots, and in this way – the quantity N of the exponential functions in (2.2), depend on the order of the partial differential equation of motion of the spectral finite element. These exponential functions are multiplied by arbitrary constants A_{nm}, which are determined by the boundary conditions formulated for the spectral finite element. The boundary conditions for the spectral finite element with an imperfection consist, in general, of the internal dynamic boundary conditions describing equilibrium of internal forces and moments in the cross-section, in which this imperfection has been assumed, as well as of the external geometric boundary conditions in the form of unknown nodal translational and rotational displacements. Then,

the mentioned arbitrary constant coefficients, and in this way also the eigen-functions of the spectral finite element (2.2), are determined as functions of the unknown nodal displacements. The spectral finite element nodal loads in the form of nodal forces and moments can be determined by means of proper differentiations of the eigenfunction with respect to the spatial co-ordinate x. Here, the nodal loads become also functions of the unknown nodal displacements, according to the general formulation for the finite element method:

$$(2.3) \qquad \{F\} = [K(\omega)]\{q\},$$

where $\{F\}$ and $\{q\}$ denote respectively the vectors of nodal loads and nodal displacements, and $[K(\omega)]$ is the angular frequency-dependent stiffness matrix of the spectral finite element, which in the case of a 2-node rod spectral element can be expressed in the following form, [1]:

$$(2.4) \quad K(\omega) = \frac{EA}{L}\frac{ikL}{(1-e^{-i2kL})}\begin{bmatrix} 1+e^{-i2kL} & -2e^{-ikL} \\ -2e^{-ikL} & 1+e^{-i2kL} \end{bmatrix}, \qquad k = \omega\sqrt{\frac{\rho}{E}},$$

where E denotes Young's modulus, A is the area of rod cross-section, ρ denotes the material density and L is the length of the rod spectral element.

In order to investigate the wave propagation processes in the spectral finite element, the dynamic analysis is carried out first in the frequency domain. Then, to the properly constrained spectral finite element an additional, so-called, "throw-off" spectral finite element is attached to the selected unclamped extreme cross-section, [1–9]. The main tasks of the "throw-off" elements are: to exclude the effect of reflection of waves at the boundaries, to filter any noise artificially from near-field response for accurate estimation and to allow the absorption or leakage of energy to simulate the damped response of a real structure. The models of tested complex structures can be partitioned into local and remote parts, and the mutual connections can be replaced with the throw-off elements that conduct the energy out of the local substructure. The throw-off spectral element is characterized by at least one infinite dimension, which in its stiffness matrix results in tending to zero of the selected terms corresponding to the reflected wave propagation. For example, the 2-node rod spectral element becomes a 1-node element, when the length L of which tends to infinity. Then, expression (2.4) describing its stiffness matrix reduces to

$$(2.5) \qquad K_{\text{off}}(\omega) = EA\,[ik], \qquad k = \omega\sqrt{\frac{\rho}{E}}.$$

Next, it is necessary to determine the stiffness matrix in the form of a frequency response function of the assembly of the main constrained spectral finite

element and the "throw-off" spectral element. Here, the upper bound of the frequency range corresponds to the Nyquist frequency of the FFT analysis of the actual diagnostic impulse $P(t)$, which is going to be imposed on the spectral element to excite the wave propagation process. The spectral response in frequency domain due to the assumed diagnostic signal $P(t)$ imposed on the considered system, is obtained by convolution of the inverse of the global stiffness matrix with the amplitude spectrum of $P(t)$. The dynamic response in time domain of the system modelled by means of the spectral finite element method is finally determined by the Inverse Fast Fourier Transformation (IFFT) of the response in frequency domain, [1–9].

3. Characterization of the method based on the visco-elastic continuous macro-elements (V-ECM)

The method of a discrete-continuous modelling of mechanical systems, which is based on the visco-elastic continuous macro-elements, has been described in details in the dissertation [10] and applied e.g. in [10–17]. This approach seems to be a universal tool for studying dynamic phenomena. In a contradistinction to the finite element method, the structural visco-elastic continuous macro-elements defined in [10] and applied in [10–17] are characterized by a natural continuous distribution of the inertial visco-elastic properties, which enables us to investigate low- and high-frequency dynamic processes as well as the wave effects. Because each continuous macro-element has an infinite number of degrees of freedom, using the analytical local solutions of the partial differential equation of its motion, theoretically there is no problem of the upper bound of the studied vibration frequency as in the case of classical finite element formulation, where this limit depends on the discretization mesh density.

Since the respectively identical partial differential equations of motion of the spectral finite elements and of the visco-elastic continuous macro-elements are solved analytically with the assumed dynamic and geometrical boundary conditions, both approaches are characterized by some kind of similarity. It is the case in the introductory step of the problem formulation and only when the separation of variables method is used as a solution for the visco-elastic continuous macro-elements, [10, 13–17]. In reality, wave solutions (2.1) applied for the spectral finite elements, reduce to the separation of variables method, what leads to the same forms of characteristic equations of the partial differential motion equations as these for the visco-elastic continuous macro-elements. Thus, respectively identical forms of eigenfunctions for the spectral finite elements and for the visco-elastic continuous macro-elements are obtained. Because the spectral finite elements are mostly applied for investigation of wave effects, the successive terms in their eigenfunctions are of exponential form (2.2), [1–9].

However, in the case of visco-elastic continuous macro-elements, these exponential terms are substituted by the harmonic and hyperbolic functions, which are more convenient for the eigenproblem analyses, [10, 13–17]. Moreover, the arbitrary constants appearing in the eigenfunction of the visco-elastic continuous macro-elements are determined by solving the eigenvalue problem with the boundary conditions formulated for the constrained system, but not as functions of nodal displacements, as in the case of the spectral finite elements. The successive important difference between mathematical formulations of the problem for both the compared approaches is that each eigenfunction of the visco-elastic continuous macro-element, or of a combination of the visco-elastic continuous macro-elements in a discrete-continuous model, corresponds to respective natural frequency of the considered mechanical system. However, the eigenfunctions of the spectral finite elements play a role of their shape functions and they correspond to current frequencies of the studied actual vibration process, [1–9].

4. Formulation of the problem for crack detection in the cantilever rod

Because of a naturally spectral character of the visco-elastic continuous macro-elements caused by continuous distribution of their inertial-visco-elastic properties, these macro-elements can be used for studying the wave propagation processes in cracked rods, shafts and beams in an analogous way as by means of the spectral finite elements. It will be demonstrated in the first comparative example for the investigated in [3] cracked cantilever rod of the total length $l = 2$ m, square cross-section of the size $a = 0.02$ m and of the crack depth equal to 5% of the rod height. The dynamic model of this rod is presented in Fig. 1. In this rod a transverse crack is assumed in the middle of its length, i.e. in the cross-section of the spatial co-ordinate $x = l_1 = 0.5l$. An additional flexibility caused by this crack is represented by the massless spring connecting the left-hand side part of the rod with its right-hand side part, as shown in Fig. 1. The longitudinal stiffness value k_o of this spring has been determined in the same way as in [3, 5], i.e. by means of the Castigliano theorem using fundamentals of the fracture mechanics. In the case of the rod considered $k_o = 1.0425 \cdot 10^{12}$ N/m.
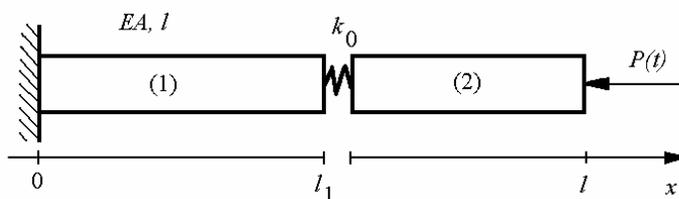
FIG. 1. Discrete-continuous model of the cracked cantilever rod built by means of the visco-elastic continuous macro-elements (V-ECM)

The cracked cantilever rod is represented by two longitudinally deformable visco-elastic continuous macro-elements (1) and (2), Fig. 1. Motion of their cross-sections is described by the following homogeneous partial differential equations:

$$(4.1) \qquad \Gamma \left(1 + \tau \frac{\partial}{\partial t}\right) \frac{\partial^2 u_i(x,t)}{\partial x^2} - \mu \frac{\partial^2 u_i(x,t)}{\partial t^2} = 0, \qquad i = 1, 2,$$

where $\Gamma = E$ is Young's modulus, $\mu = \rho$ denotes the material density, $u_i(x,t)$ are the longitudinal displacements of rod cross-sections and τ denotes the retardation time of the Kelvin–Voigt model of material damping. Equations of motion (4.1) are solved with the following boundary conditions:

$$(4.2)_1 \qquad u_1(x,t) = 0 \qquad \text{for} \quad x = 0$$

$$\text{(in the case of rod spectral finite element} \quad u_1(0,t) = \hat{q}_1),$$

$$(4.2)_2 \qquad u_1(x,t) = u_2(x,t) \qquad \text{(without crack)} \quad \text{or}$$

$$EA \frac{\partial u_1(x,t)}{\partial x} = k_0 \left(u_2(x,t) - u_1(x,t)\right) \qquad \text{(with crack)}$$

and

$$(4.2)_3 \qquad \frac{\partial u_1(x,t)}{\partial x} = \frac{\partial u_2(x,t)}{\partial x} \qquad \text{for} \quad x = l_1,$$

$$(4.2)_4 \qquad EA \frac{\partial u_2(x,t)}{\partial x} = P(t) \qquad \text{for} \quad x = l$$

$$\text{(in the case of rod spectral finite element} \quad u_2(l,t) = \hat{q}_2),$$

where $A = a^2$ denotes the area of the rod cross-section, $P(t)$ is the longitudinal external force yielding the diagnostic impulse in order to excite wave propagation processes and $\hat{q}_1$, $\hat{q}_2$ denote the nodal longitudinal displacements of the analogous, cracked spectral finite element discussed in [3].

An application of the separation of variables solution to Eqs. (4.1) results in the analytical form of eigenfunctions for both macro-elements, [10, 13–16]

$$(4.3) \qquad U_i(x) = B_{1i} \sin\left(\frac{\omega}{\nu}x\right) + B_{2i} \cos\left(\frac{\omega}{\nu}x\right) \qquad \text{where} \ \ 0 \leq x \leq l_1 \ \text{ for } \ i = 1$$

$$\text{and} \ \ l_1 \leq x \leq l \ \text{ for } \ i = 2.$$

Here, $\nu = \sqrt{\Gamma/\mu} = \sqrt{E/\rho}$ denotes the longitudinal wave propagation velocity. The eigenfrequencies ω corresponding to orthogonal eigenfunctions (4.3)

are determined from the following characteristic equation of the formulated in this way, implicit eigenvalue problem for the considered cracked cantilever rod

$$(4.4) \qquad \mathbf{A}(\omega) \cdot \mathbf{B} = \mathbf{0},$$

where $\mathbf{A}(\omega)$ denotes the characteristic matrix expressed as a function of the natural frequency ω and $\mathbf{B}$ is the vector of the arbitrary coefficients appearing in eigenfuctions (4.3) and mentioned in Secs. 2 and 3. The successive natural frequencies of the considered structure $\omega_1, \omega_2, \omega_3,...$ are roots of the determinant of the characteristic matrix $\mathbf{A}(\omega)$. The eigenfunctions corresponding to these frequencies are obtained by solving algebraic equations (4.4), i.e. by a computation of the unknown coefficients in vector $\mathbf{B}$, for the successive values $\omega_1, \omega_2, \omega_3,...$ regarded here as parameters.

The natural spectral character of the visco-elastic continuous macro-elements (V-ECM) mentioned above, enables us to obtain the system dynamic response directly in the time domain due to an assumed diagnostic impulse, contrary to the spectral finite element method, in the case of which the system amplitude spectrum and then the response in the frequency domain must be determined first before the IFFT. Thus, in order to obtain the dynamic response in the time domain by means of the visco-elastic continuous macro-elements, the analytical Fourier solution of motion equations (4.1) is applied in the form of series of the orthogonal eigenfunctions $U_{im}(x)$

$$(4.5) \qquad u_i(x,t) = \sum_{m=1}^{\infty} U_{im}(x)\xi_m(t), \qquad i = 1, 2.$$

Upon an analytical determination of the modal masses γ_m^2 corresponding to the successive natural frequencies ω_m, according to [10, 13–18], the Fourier solution (4.5) leads to the following ordinary differential equations in modal co-ordinates $\xi_m(t)$

$$(4.6) \qquad \ddot{\xi}_m(t) + \tau\omega_m^2\dot{\xi}_m(t) + \omega_m^2\xi_m(t) = \frac{U_{2m}(l)}{\gamma_m^2}P(t), \qquad m = 1, 2, ..., N,$$

where $U_{2m}(l)$ denotes the value of the m-th eigenfunction for the rod free cross-section $x = l$, on which the diagnostic longitudinal concentrated force $P(t)$ is applied, as shown in Fig. 1. Integer N is the number of the eigenmodes taken into consideration in the series (4.5).

In order to study the wave propagation processes by means of the spectral finite element method (SFEM) as well as using the discrete-continuous models
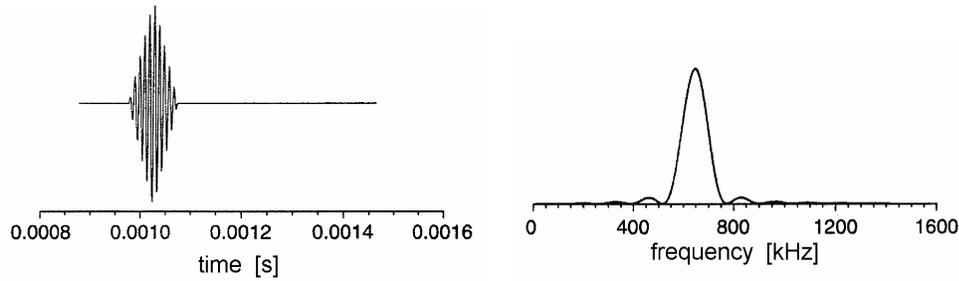
FIG. 2. Diagnostic impulse in time and frequency domain applied in [3, 5, 6, 8, 9].

and the visco-elastic continuous macro-elements (V-ECM), the triangular impulse modulated by the high-frequency sinusoid seems to be very convenient, as the diagnostic excitation force $P(t)$. In Fig. 2, in the time and frequency domain, is shown a plot of such a function applied in [3, 5, 6, 8, 9].

In the considered non-cracked and cracked cantilever rod, was studied the longitudinal wave propagation process due to the identical as in [3, 5, 6] and depicted in Fig. 2, excitation triangular impulse $P(t)$ characterized by the total duration time of 0.0000925 s and modulated by 10 full sinusoids within this time. In order to obtain a sufficiently high accuracy of results, the time step value for a direct integration of equations (4.6) using the Newmark method has been selected equal to $1.33 \cdot 10^{-7}$ s. This value corresponds to the maximal possible frequency component of 7500 kHz of the investigated dynamic process. A relatively fast convergence of series (4.1) enabled us to truncate it above $N = 116$ eigenfunctions taken into consideration in (4.5) and (4.6), in the frequency range $0 \div 150000$ Hz for $\tau = 0$. For a greater number N of the considered eigenfunctions, any remarkable increase of accuracy of the response was not observed. Despite the relatively great number N of equations (4.6) being solved with such a small integration step value, the entire computation time of a single simulation did not exceed 5 s of an operation of the average-power PC.

The results of such simulation performed for the parameters listed above are presented in Fig. 3. The analogous results of wave propagation in the considered cracked rod obtained in [3] are shown in Fig. 4. In Fig. 3a several peaks of the longitudinal acceleration of the rod free end appear, where the "first" peak corresponds to the direct action of the external force $P(t)$ and the "next" peaks are caused by successive reflections of the longitudinal waves from the clamped and free ends of the rod. According to the well-known theory of one-dimensional elastic wave reflections from the free end of the rod, all these "next" peaks have two times greater extreme values than the "first" peak. It should be noted that in the case of analogous simulation performed for the identical cracked rod in [3]

by means of the spectral finite element method (SFEM), only two acceleration peaks of comparable extreme values occurred, see Fig. 4a. This essential difference is explained by application of the throw-off spectral element attached to the free end of the spectral element representing the cracked rod. This throw-off element plays a role of the waveguide "swallowing" all the reflected waves from the clamped end of the rod. In the case of a cracked rod, in Fig. 3b as well as in Fig. 4b between the "big" peaks, due to wave reflections from the rod ends, several additional very small peaks have occurred, which are almost invisible in the presented scale. These small peaks appear regularly after successive wave

a)

b)

c)
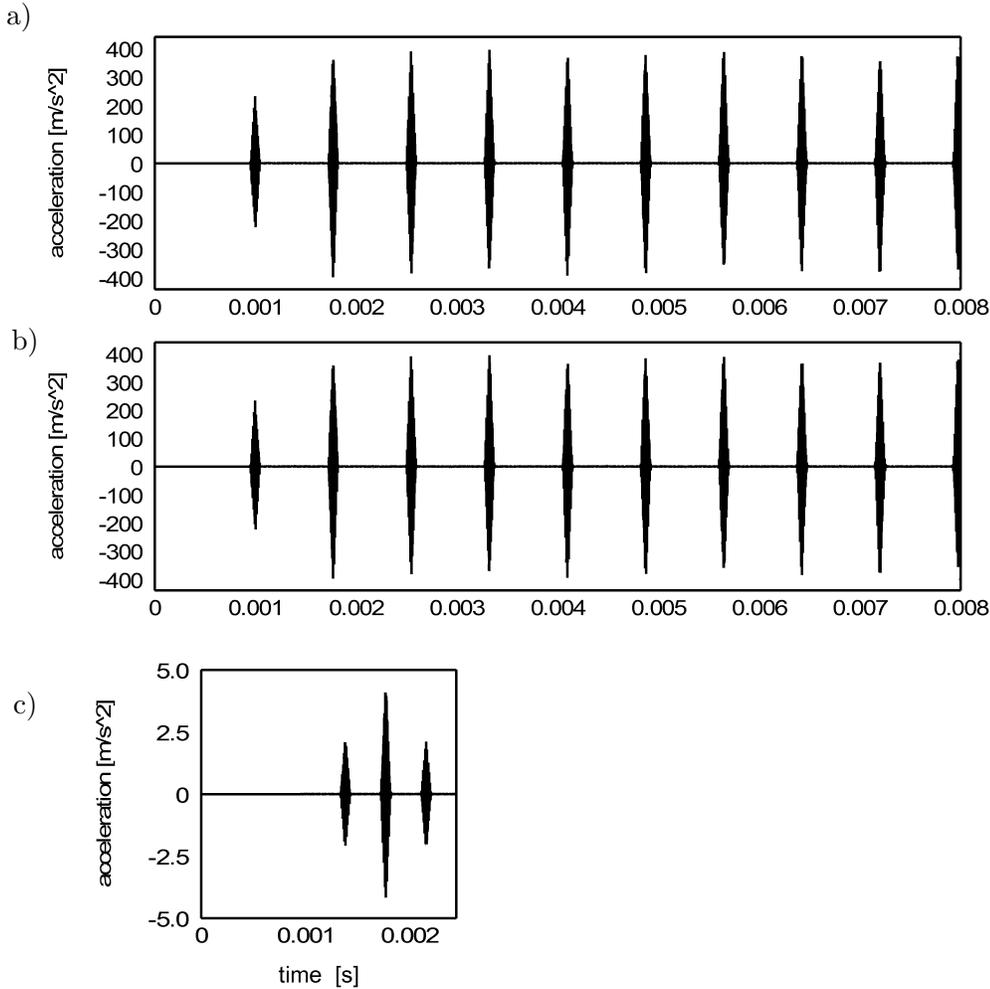
FIG. 3. Acceleration of the rod free end obtained by means of the V-ECM and the Fourier solution.

reflections from the rod cross-section, in which the crack has been assumed. Such three first peaks are shown in Figs. 3c and 4c, demonstrating the algebraic difference between the responses of the rod with the crack and without the crack. The first peaks in Figs. 3c and 4c, are a result of the wave reflection from the cracked cross-section and caused by the acceleration wave propagating towards the rod clamped end. The second peaks are the differences of the waves reflected from the rod clamped end for the cracked and non-cracked rod. The third peaks in Figs. 3c and 4c are also a result of the wave reflection from the cracked cross-section, but caused by the acceleration wave reflected from the clamped end.
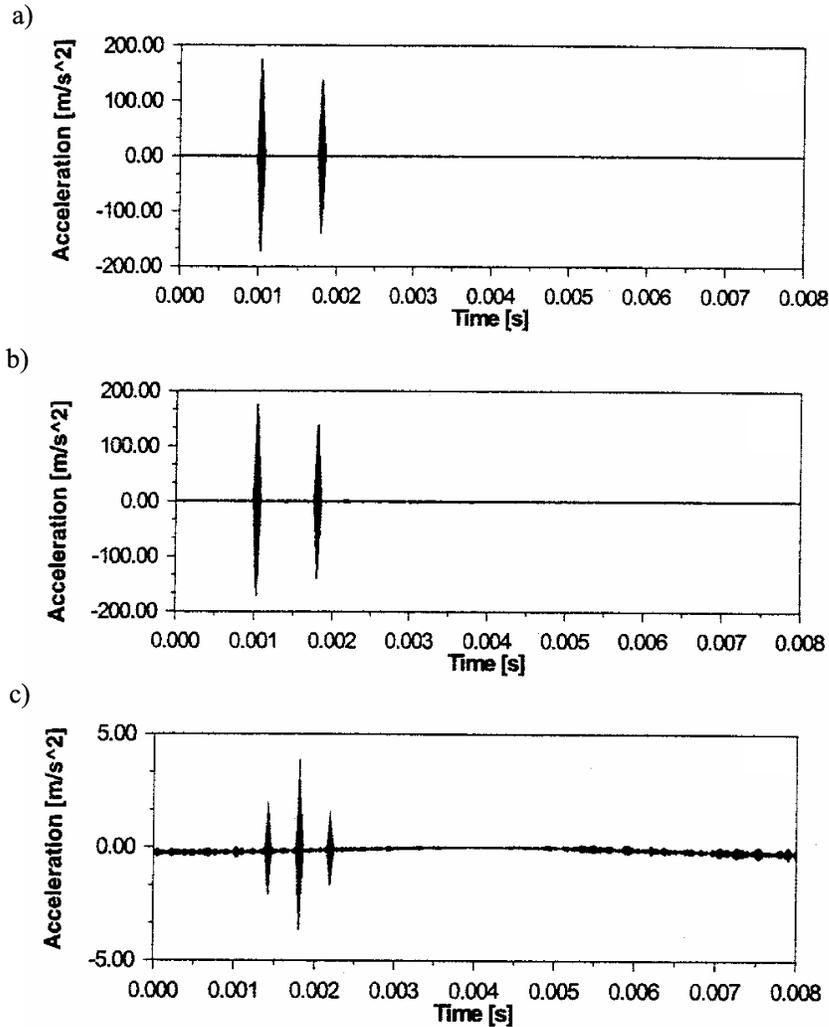
FIG. 4. Acceleration of the free end of the rod obtained by means of the SFEM in [3].

Appearance of these additional reflected waves informs us about the existence of an imperfection. Here, the known value of wave propagation velocity multiplied by the proper time delay corresponding to instants of appearance of these additional waves reflected from the crack, enables us to localize this imperfection in the considered continuous medium. The result depicted in Fig. 3c is very similar to the analogous one in Fig. 4c obtained in [3]. This similarity follows from the very small mutual differences of the respective response values corresponding to the same successive time instants. These differences are not greater than $2 \div 3\%$, which is negligible from the viewpoint of the postulated research target using the two compared methods. Thus, it is to conclude that by means of the visco-elastic continuous macro-elements (V-ECM) and the Fourier solution (4.5) of motion equations (4.1), a crack detection and localization can be performed directly in the time domain – similarly as in the case of using the spectral finite element method (SFEM), but first – in the frequency domain and then – in the time domain.

Crack detection and localization in elastic rods can be also carried out by means of the elastic continuous macro-elements using the d'Alembert wave solutions of motion equations (4.1) for $\tau = 0$ in the following form:

$$(4.7) \qquad u_i(x,t) = f_i\Big(\nu(t - t_{0i}) + x - x_{0i}\Big) + g_i\Big(\nu(t - t_{0i}) - x + x_{0i}\Big)$$

$$i = 1, 2, \quad \nu = \sqrt{\Gamma/\mu} = \sqrt{E/\rho}.$$

Functions f_i and g_i represent longitudinal waves caused by the excitation impulse $P(t)$, where the function f_i represents a longitudinal wave propagating in the i-th continuous macro-element along the x-axis negative sense, Fig. 1; however, the function g_i represents a longitudinal wave propagating along the x-axis positive sense and ν denotes the wave propagation velocity. According to the one-dimensional wave propagation theory, it is taken into account in (4.7) that the first perturbation in the i-th macro-element occurs in the cross-section of the co-ordinate x_{0i} after the finite time delay t_{0i}. Furthermore, it is assumed that the functions f_i and g_i are continuous and are null for negative arguments, i.e. before arrival of the first perturbation.

Since solutions (4.7) satisfy identically the motion equation (4.1) for $\tau = 0$, actual values of the wave functions f_i and g_i are determined by the boundary conditions of the problem. Thus, by substituting the wave solutions (4.7) into the boundary conditions (4.2), denoting the largest argument in each equation by z, and by rearranging these equations in such a way that their right-hand sides are always known, in the considered case of the rod with a constant cross-section we obtain the following system of algebraic and ordinary differential equations of the first order with a "shifted" or "retarded" argument

for the functions f_i and g_i, $i = 1, 2$:

$(4.8)_1$
$$g_1(z) = -f_1(z - 2l_1),$$
$$g_2(z) = -f_2(z - 2l_2) + f_1(z - l_2) + g_1(z - l_2),$$

$(4.8)_2$
$$f_1'(z) = f_2'(z - l_2), \qquad \text{(without crack)}$$

$(4.8)_3$
$$\begin{bmatrix} 1 & 0 \\ 0 & 1 \end{bmatrix} \begin{bmatrix} g_2'(z + l_2) \\ f_1'(z) \end{bmatrix} + \begin{bmatrix} \tilde{K} & -\tilde{K} \\ -\tilde{K} & \tilde{K} \end{bmatrix} \begin{bmatrix} g_2(z + l_2) \\ f_1(z) \end{bmatrix}$$

$$= \begin{bmatrix} f_2'(z - l_2) + \tilde{K} \left[g_1(z) - f_2(z - l_2) \right] \\ g_1'(z) - \tilde{K} \left[g_1(z) - f_2(z - l_2) \right] \end{bmatrix},$$

(with crack)

$(4.8)_4$
$$f_2'(z) = \tilde{P}(z) + g_2'(z),$$

where: $\tilde{K} = \dfrac{k_0 \, l_s}{EA}$, $\quad \tilde{P}(z) = \dfrac{P(t) \, l_s}{EA}$, $\quad l_2 = l - l_1$, and l_s is the reference distance.

The above equations have been solved numerically by means of the Newmark method using the appropriately small direct integration step, in order to obtain a sufficient accuracy of the results of simulation of the high-frequency dynamic process. The right-hand sides of the equations with a shifted argument, which are known after each integration step, similarly as in [10–12], enable us to solve these equations one after another, i.e. in the sequence defined here by (4.8).

The dynamic response shown in Fig. 5a and obtained for the non-cracked rod using the d'Alembert solutions (4.7) and equations (4.8), is almost identical with that determined by means of the Fourier solution (4.5) and illustrated in Fig. 3a. The dynamic response of the cracked rod and the difference between the responses obtained for the cracked and non-cracked rod using relations (4.7) and (4.8), are depicted in Figs. 5b and 5c, respectively. Between the "big" peaks due to wave reflections from the rod ends in Fig. 5b, similarly as in Fig. 3b, we can observe very small peaks of the longitudinal acceleration caused by the successive elastic wave reflections from the rod cross-section, in which the crack has been assumed. The first three peaks of the difference of the longitudinal acceleration of the rod free end, presented in Fig. 5c, are almost identical with those depicted in Fig. 3c, for which the Fourier solution (4.5) has been used. According to the above, both applied analytical solutions enable us to achieve the assumed

research target with almost the same computational accuracy and efficiency. This fact confirms in this way a reliability of the proposed method based on the V-ECM. Moreover, both differences are very similar to the analogous difference obtained in [3] by means of the spectral finite elements and shown in Fig. 4c, where the mutual discrepancies of respective response values in successive time instants do not exceed 3%.
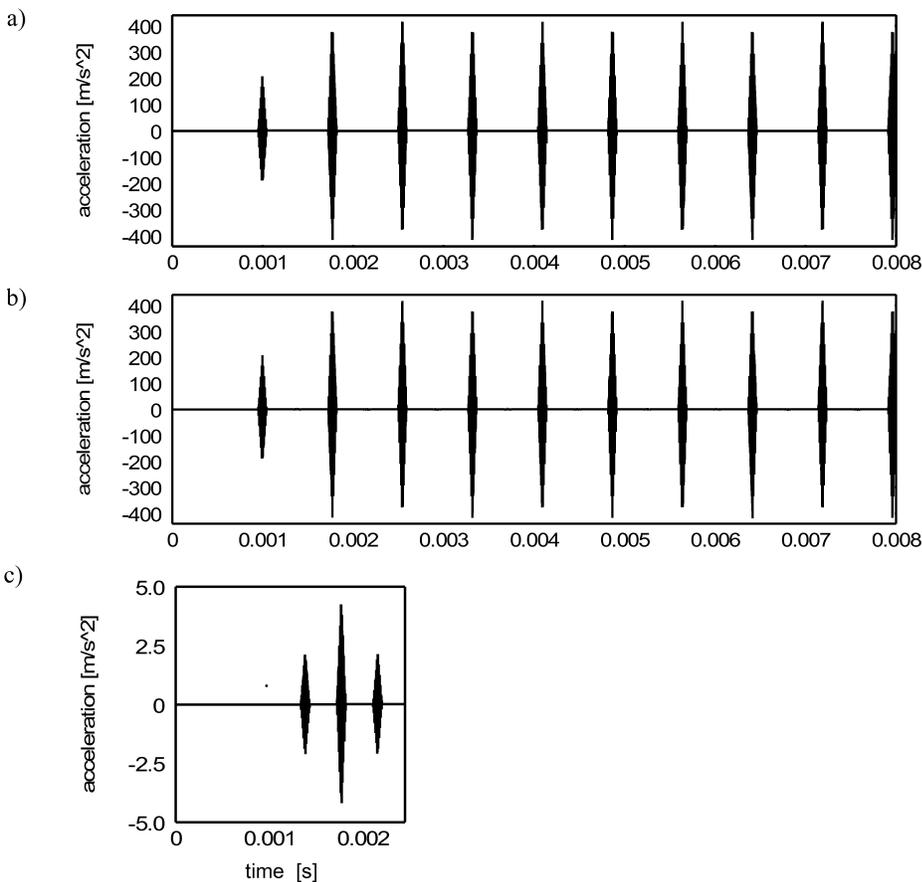
Fig. 5. Acceleration of the rod free end obtained by means of the V-ECM and the d'Alembert solution.

Moreover, it is to emphasize that, as it follows from [10–17] as well as from the dissertation [19], by means of the applied two solutions, i.e. the Fourier solution (4.5) and the d'Alembert solution (4.7) of motion equations (4.1), also torsional elastic wave propagation due to torsional diagnostic excitation can be investigated. In this way, several imperfections in machine shafts and vehicle axles could be detected and localized as well.

5. Formulation of the problem of crack detection in the cantilever beam

An analogous investigation using the method of discrete-continuous modelling based on the visco-elastic continuous macro-elements (V-ECM) can be performed for the cantilever beam with a transverse crack considered in [5, 8, 9], or for the beam with a local delamination studied in [4, 6]. The dynamic model of the cracked beam is shown in Fig. 6. It is known that the beam has in general a dispersive character of wave propagation, what results in decaying of the high-frequency waves in space and in time, [1]. This feature makes troublesome the detection and localization of defects in the beam. The sole exception here is the so-called "second frequency band" of the Timoshenko beam. In this range of frequencies, only spatially non-damped shear and longitudinal waves propagate in the beam, similarly to the longitudinal waves in rods and torsional waves in shafts, [1, 20–22]. For each Timoshenko beam this second frequency band exists above the proper so-called "cut-off frequency" equal to $\omega_c = \sqrt{(sGA/\rho I)}$, where A and I denote respectively the beam cross-sectional area and the geometric moment of inertia, s is the Timoshenko beam shear ratio and G and ρ denote Kirchhoff's modulus and the material density. Since in the publications devoted to an application of the spectral finite elements for dynamic investigation of beams, e.g. in [2, 4–6, 8, 9], there is no information about distinguishing of the first and the second frequency bands in the Timoshenko beam eigenfrequency range, one can suppose that in the mentioned papers, the Timoshenko beam has been *a priori* regarded as a waveguide for spatially non-damped waves only. This corroboration follows from the fact that in [4–6, 9] all four roots k_n, $n = 1, 2, \ldots, N = 4$, in (2.2) of the characteristic equation for the Timoshenko beam are assumed to be always imaginary. Moreover, the computational results obtained in these works indicate a typical character of shear waves propagating in the beam with the velocity $\sqrt{(sG/\rho)}$, i.e. similarly to the Flügge beam described in [20–22].
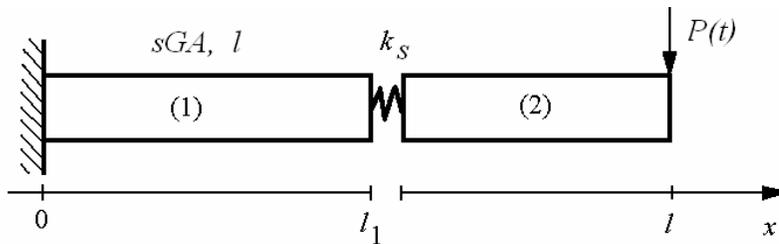
FIG. 6. Discrete-continuous model of the cracked cantilever beam built by means of the visco-elastic continuous macro-elements.

According to the above, the Timoshenko-beam visco-elastic continuous macro-element defined in [10] can be also regarded as an analogous waveguide, the cross-sections of which are affected only by shear deformations propagating in the form of a front of discontinuity due to transverse high-frequency or impulse-like external excitations. Such simplification has been substantiated in [20–22] as well as in [19] by means of the proper comparison of natural frequencies of the classical Timoshenko beam, with respective shear beam eigenfrequencies corresponding to wave lengths smaller than the beam height. Thus, according to [19, 20], the equation of motion of the Timoshenko beam can be reduced to wave equation (4.1). Then, an investigation of the same as in [5] problem of wave propagation in the cracked cantilever beam under the diagnostic, concentrated external transverse force imposed on the beam free end reduces to solving equations (4.1) for $\Gamma = sG$ and $\mu = \rho$ with the boundary conditions (4.2). Here, the longitudinal displacements of the rod cross-sections $u_i(x,t)$, $i = 1,2$, become the transverse displacements of the shear-beam cross-sections, Young's modulus E is replaced by the product sG, and the longitudinal component of the crack stiffness k_o determined by means of the Castigliano theorem is replaced by the proper transverse component k_S of the crack local stiffness matrix. Further steps of the mathematical formulation of the problem for the cracked shear-beam shown in Fig. 6 are the same as those for the cracked rod expressed by formulae (4.3)÷(4.6) using the Fourier solution of motion equations (4.1), or by formulae (4.7)÷(4.8) by means of the d'Alembert solution of (4.1).

In the computational example there is considered the identical as in [5] – cracked cantilever beam of the entire length $l = 2$ m, height 0.02 m, width 0.02 m and the crack depth equal to 20% of the beam height. Here, the numerical value of the crack stiffness k_S is equal to $2.0 \cdot 10^{10}$ N/m. The beam is excited by the transverse concentrated force $P(t)$ imposed to its free end. The time history of this force in the form of diagnostic triangular impulse characterized by the total duration time of 0.000185 s and modulated by 10 full sinusoids within this time is depicted in Fig. 2. Here, Eqs. (4.6) were solved using the Newmark method with the direct integration time-step value equal to $1.0 \cdot 10^{-7}$ s, which corresponds to the maximal possible frequency component of 10000 kHz of the investigated dynamic process. In comparison with the studied above longitudinal waves propagating in the cantilever rod, in this case it was necessary to take into consideration $N = 269$ modal Eqs. (4.6) in the frequency range $0 \div 200000$ Hz for $\tau = 0$, in order to achieve entirely satisfactory convergence of the simulation results obtained by means of series (4.5).

In Figs. 7, 9 and 11 are presented the simulation results of shear wave propagation in the form of transverse displacements of a cantilever cracked beam. Analogous results obtained in [5] for the considered beam are shown respectively in Figs. 8, 10 and 12. Figures 7 and 8 demonstrate the time histories of

the shear wave propagation in the beam, in which the crack has been assumed at the distance equal to 25% of the beam entire length l from its clamped end, i.e. for $x = l_1 = 0.25l$. In these figures are observed "big" displacement peaks caused directly by the diagnostic impulse and by the shear wave reflections from the beam ends, as well as small but remarkable peaks due to wave reflections from the cracked cross-section $x = l_1$. In Figs. 7a and 8a, the plot of transverse displacement of the beam free end is shown and in Figs. 7b, 8b and in 7c, 8c there are presented plots of transverse displacement of the cross-sections at the distance of respectively $0.3l$ and $0.7l$ from the free end of the beam. In turn, in Figs. 9, 10 and in Figs. 11, 12 are depicted analogous time histories of transverse displacements of the beam free end, where the crack has been assumed to be in the cross-section located in the center of the beam, i.e. for $x = l_1 = 0.5l$, and
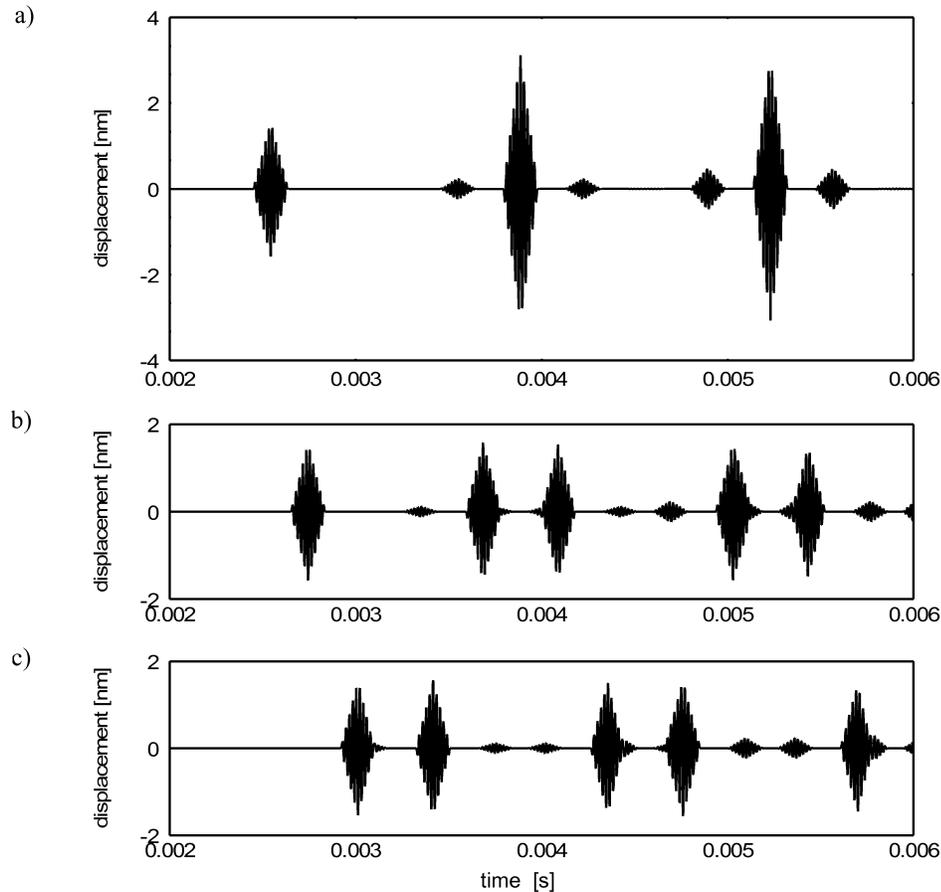
FIG. 7. Shear wave propagation in the cantilever beam with the crack in the cross-section located at the distance of 25% of the beam length from its clamped end (obtained using the V-ECM).
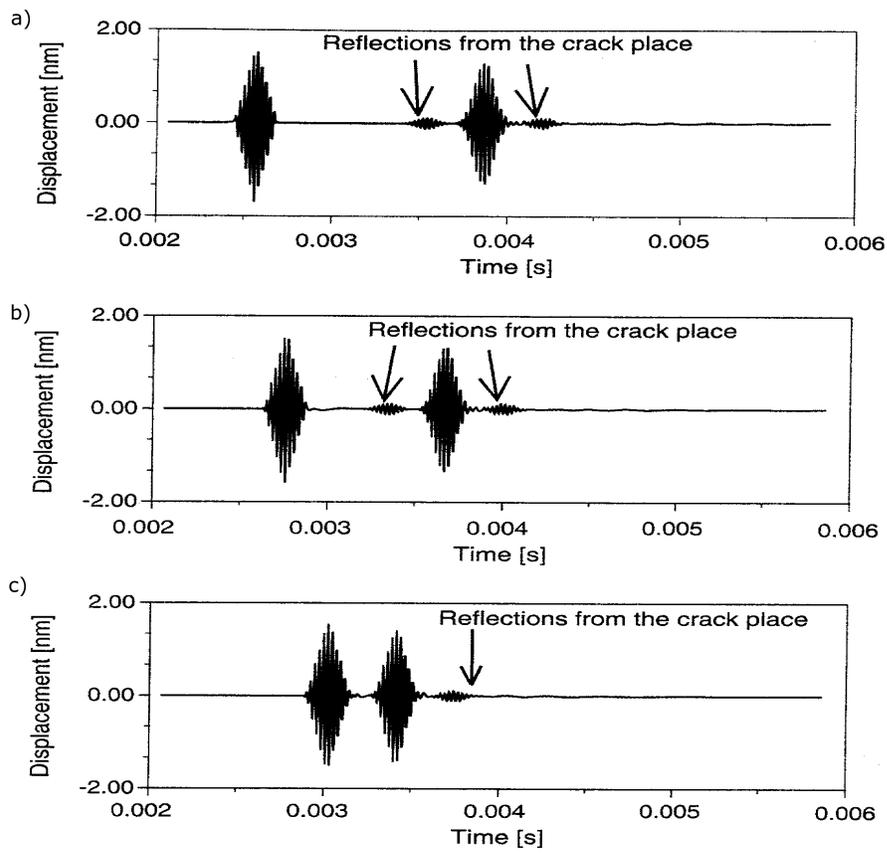
FIG. 8. Shear wave propagation in the cantilever beam with the crack in the cross-section located at the distance of 25% of the beam length from its clamped end (obtained in [5] using the SFEM).
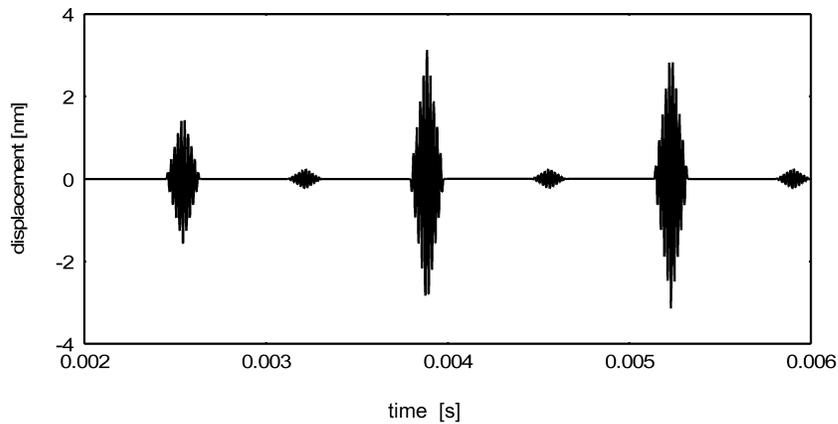
FIG. 9. Transverse displacement of the free end of the cantilever beam with a crack in the middle of its entire length (obtained using the V-ECM).

75% of the beam length, i.e. for $x = l_1 = 0.75l$, from its clamped end. From the viewpoint of crack detection and localization, all results obtained using the visco-elastic continuous macro-elements (V-ECM) in time domain and presented in Figs. 7, 9 and 11 are almost identical to these shown in Figs. 8, 10 and 12, determined in [5] by means of the spectral finite element method (SFEM). Here, the most important similarity criterion is not the above-mentioned difference of the respective response values, but first of all – almost the same time instants, at which the waves reflected from the crack occur. Some remarkable differences of the corresponding plots are caused in the case of the spectral finite element method by the throw-off waveguide, excluding the effects of wave reflections from the beam free end. The lack of such a waveguide in the discrete-continuous model built by means of the visco-elastic continuous macro-elements results in two times bigger extreme values of the transverse displacements yielded by shear wave reflections from the beam free end as well as in the multiple wave reflec-
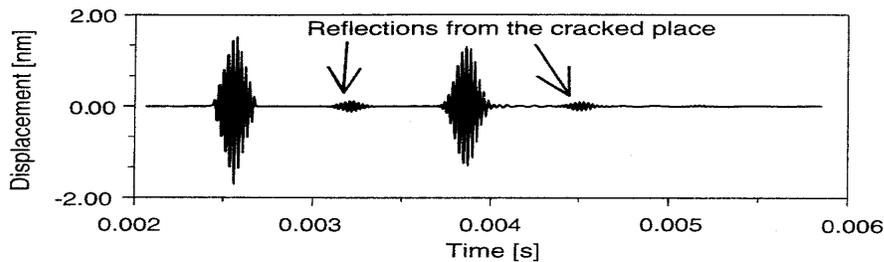
Fig. 10. Transverse displacement of the free end of the cantilever beam with a crack in the middle of its entire length (obtained in [5] using the SFEM).
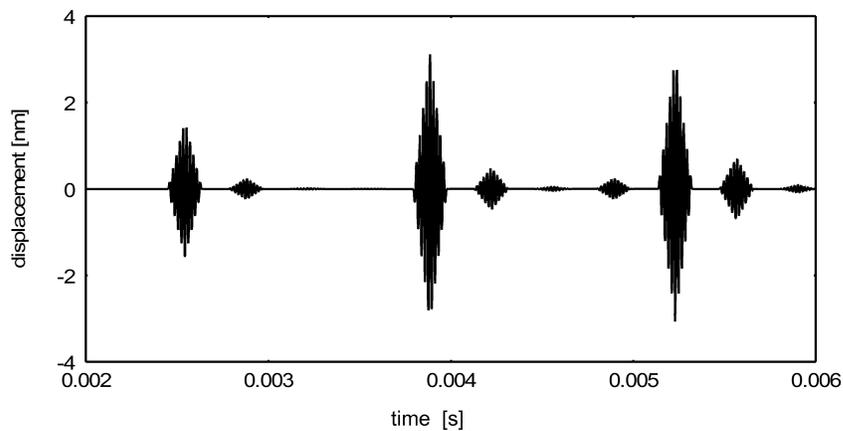
Fig. 11. Transverse displacement of the free end of the cantilever beam with a crack in the cross-section located at the distance of 75% of the entire length from the clamped end (obtained using the V-ECM).
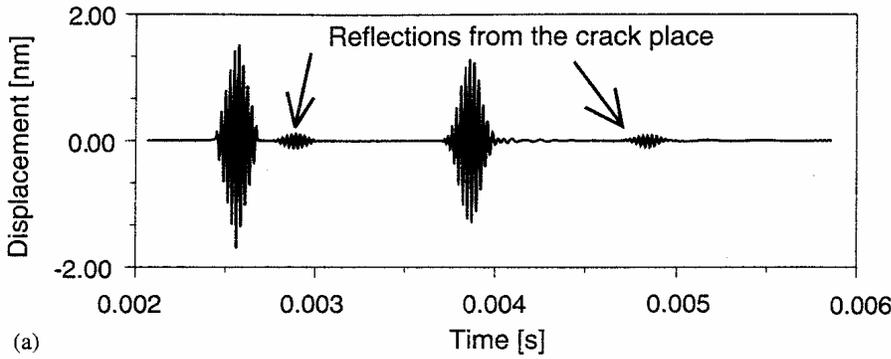
FIG. 12. Transverse displacement of the free end of the cantilever beam with a crack in the
cross-section located at the distance of 75% of the entire length from the clamped end
(obtained in [5] using the SFEM).

tions in time from both beam ends and from the cross-section, in which the
crack has been assumed.

Very similar results to these demonstrated in Figs. 7, 9 and 11 have been ob-
tained using the d'Alembert solution (4.7) of motion equations (4.1) for
$\Gamma = sG$ and $\mu = \rho$, with the boundary conditions (4.2), by means of sequential
solving of the algebraic and ordinary differential equations (4.8) with a retarded
argument.

6. The continuous throw-off macro-element

All cases of the cantilever rod and shear beam studied above in Sec. 4 and
5 have been investigated without any throw-off elements mentioned in Sec. 2
for the spectral finite elements. From the viewpoint of crack detection, in the
considered examples an application of an additional element conducting the
reflected diagnostic waves out was not particularly important. Moreover, an
observation of systematically propagating and reflecting waves enabled us to
evaluate and demonstrate the computational accuracy and numerical stability of
the applied algorithms, based on analytical Fourier's and d'Alembert's solution
of motion Eqs. (4.1) for the continuous elastic macro-elements. Nevertheless,
because of the reasons mentioned in Sec. 2, it is necessary to introduce the
throw-off element into the structures tested by means of the V-ECM.

In the proposed approach, an additional elastic continuous rod- or beam
macro-element of infinite length will be used in order to remove the energy out
from the tested structure. This, so-called, "continuous throw-off macro-element"
(3) can be attached to the free end of the studied above cantilever rod or shear
beam, as shown in Fig. 13. This macro-element is characterized by the same
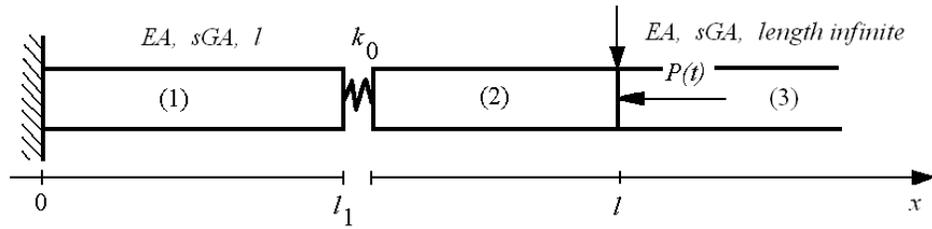
FIG. 13. Discrete-continuous model of the cracked cantilever rod or beam with the elastic continuous throw-off macro-element.

cross-sectional dimensions and material constants as the cracked rod or beam. Motion of its cross-section is described by Eq. (4.1) for $i = 3$ with the boundary conditions (4.2), where only condition (4.2_4) has to be modified to the following form:

$$(6.1) \qquad \Gamma A \frac{\partial u_2(x,t)}{\partial x} = P(t) + \Gamma A \frac{\partial u_3(x,t)}{\partial x}$$

$$\text{and} \quad u_2(x,t) = u_3(x,t) \quad \text{for} \quad x = l,$$

where $\Gamma = E$ or sG and $u_3(x,t)$ are respectively the longitudinal or transverse displacement of cross-sections of the throw-off rod or shear-beam. In order to simulate energy conduction out of the structure, the d'Alembert wave solution of motion Eq. (4.1) seems to be particularly convenient. But in this solution the wave propagation in one direction only must be assumed. Thus, this solution takes the simplified form

$$(6.2) \qquad u_3(x,t) = g_3\left(\nu(t - t_{03}) - x + x_{03}\right), \qquad \nu = \sqrt{\Gamma/\rho},$$

where g_3 represents a longitudinal or shear wave, caused by the excitation impulse $P(t)$ and propagating in the throw-off continuous macro-element along the x-axis positive sense, Fig. 13, and ν denotes the wave propagation velocity. Similarly to (4.7), according to the one-dimensional wave propagation theory, it has been taken into account in (6.2) that the first perturbation in this macro-element occurs in the cross-section of the co-ordinate $x_{03} = l$ after the finite time delay $t_{03} = 0$. By substituting the wave solution (6.2) into the boundary conditions (6.1), denoting the largest argument in each equation by z and upon eliminating function g_3, the ordinary differential equation (4.8_4) is then modified to the following form:

$$(6.3) \qquad f_2'(z) = \frac{1}{2}\tilde{P}(z),$$

where all remaining ordinary differential equations (4.8) with the retarded argument remain unchanged. Relation (6.3) indicates explicitly that in the case of throw-off element application, only one half of the external energy is supplied to the system, while the second half is conducted out. Moreover, the ability of reflected wave "swallowing" by the continuous throw-off macro-element follows from the ordinary differential equation with the retarded argument $(4.8_1) - (4.8_3)$, together with relation (6.3). This task of the continuous throw-off macro-element is then demonstrated by means of the computational example made for the cantilever rod investigated in Sec. 4.

For the cantilever cracked rod with the continuous throw-off macro-element, the numerical simulation of diagnostic wave propagation has been performed in an identical way as in Section 4 for the rod without the throw-off element, i.e. for the same rod and crack parameters as well as for the identical time step of integration of equations $(4.8_1) - (4.8_3)$ together with relation (6.3). Also the obtained results are presented in an analogous form to those in Figs. 3, 4 and 5. Thus, for the longitudinal acceleration of the rod cross-section $x = l$, Fig. 14a presents the plots of time histories of diagnostic wave propagation in the non-cracked rod, in Fig. 14b diagnostic wave propagation of the cracked rod is depicted, and Fig. 14c demonstrates the difference between the above time histories obtained for the cracked and non-cracked rod. In Fig. 14a, contrary to Figs. 3a and 5a and similarly to Fig. 4a, only two acceleration peaks are observed. The first one corresponds to the direct action of the external force $P(t)$ and its magnitude is almost the same as that in Figs. 3a, 4a and 5a. The second peak in Fig. 14a corresponds to the wave reflected from the clamped end of the rod in the cross-section $x=0$. Magnitude of this peak is the same as that of the first peak, what is in agreement with the analogous result demonstrated in Fig. 4a and obtained in [3] by means of the spectral finite element method for the identical rod with the throw-off element applied. This second peak has a similar magnitude as that in [3], i.e. it is two times smaller than the respective second and next successive peaks in Figs. 3a and 5a. This fact confirms the existence of the continuous throw-off macro-element assumed in this example, where one half of external energy is conducted out of the system and the cross-section $x = l$ does not correspond to the rod free end. In the case of the cracked rod in Fig. 14b, analogous two "big" peaks as those in Fig. 14a and in Figs. 4a,b are observed. Moreover, "between" these peaks and after the second "big" peak, similarly as in Figs. 3b, 4b and in 5b, very small, almost invisible in the used scale, additional peaks have occurred, which are a result of longitudinal diagnostic wave reflections from the cracked cross-section, as described in Sec. 4. The difference of responses obtained for the cracked and non-cracked rod and depicted in Fig. 14c indicates three peaks analogous to those discussed in Sec. 4 and illustrated in Figs. 3c, 4c and 5c. It is to emphasize that since the energy has
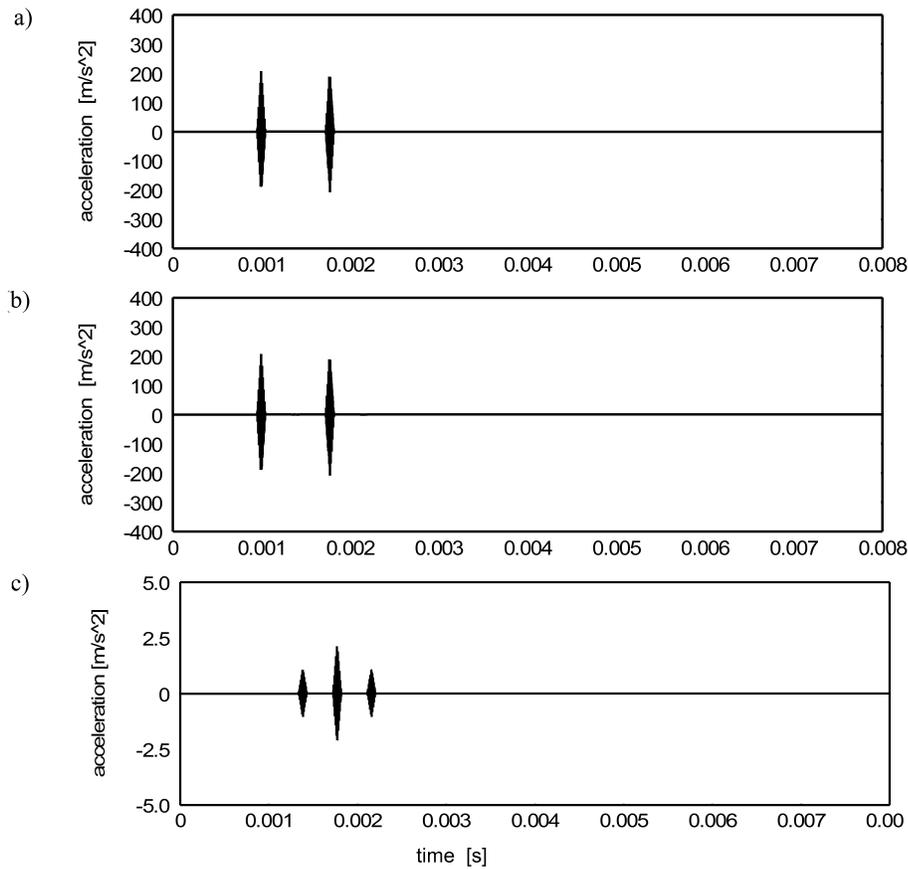
Fig. 14. Acceleration of the free end of the rod obtained using the continuous throw-off macro-element by means of the V-ECM and the d'Alembert solution.

been conducted out of the system by means of the assumed throw-off continuous macro-element, contrary to Figs. 3b, 5b and similarly to Fig. 4b, successive next reflection peaks do not occur in Figs. 14b and 14c.

The proposed continuous throw-off macro-element enabled us to obtain the effect of energy conduction out of the cantilever beam considered in Sec. 5, similar to that presented in Fig. 14.

7. Final remarks and conclusions

In the paper, the problem of crack detection and localization in the rod and beam has been considered using the discrete-continuous models based on the visco-elastic continuous macro-elements (V-ECM). Simultaneously, the ob-

tained results were compared with analogous results computed using the spectral finite element method (SFEM). The mechanical models of the cracked rod and beam applied in the case of both methods have identical structures. The only difference is caused by the assumed phenomenology of their fundamental structural elements, i.e. the spectral finite elements and the visco-elastic continuous macro-elements. Although motion of the spectral finite element is described strictly according to the given deformation theory of the considered continuous medium as well as the mathematical solution is obtained by means of analytical relations, the inertial-visco-elastic properties of this element are discretized into the form of nodal quantities, in an analogous way as that used for the classical finite element formulation. Thus, the spectral finite element frequency-dependent shape functions belonging to the class of eigenfunctions, result in frequency-dependent stiffness matrix, which must be determined in the form of frequency response function. Then, in the next step of the routine, this frequency response function must be convolved with the amplitude spectrum of the actual external excitation in order to obtain the system dynamic response in the frequency domain.

Motion of the visco-elastic continuous macro-elements (V-ECM) is also described strictly by the same equations as the motion of the spectral finite element, as well as the mathematical solution of the problem is based on analytical relationships too. However, the inertial-visco-elastic properties of the visco-elastic continuous macro-element remain continuously distributed, which assures the natural spectral character of this structural element. Thus, dynamic responses of the discrete-continuous models built by means of the visco-elastic continuous macro-elements can be obtained directly in the time domain using respectively the d'Alembert or Fourier solution of equations of motion. Moreover, the computational examples presented in this paper for the cantilever rod and beam have demonstrated a great similarity of the respective results obtained by means of the Fourier solution based on the standing wave theory with the results determined using the d'Alembert solution based on the travelling wave approach. If the d'Alembert wave solution seems to be the most convenient and natural tool of investigation of the wave effects in continuous media from the viewpoint of reliability of results, the very similar findings achieved by means of the Fourier method confirm a high value of this approach for studying the wave and high-frequency dynamic effects as well, particularly in cases, when the d'Alembert solution can not be applied.

As it follows from the above considerations, both the discussed approaches, i.e. the proposed one in the paper and the spectral finite element method, are very convenient and computationally effective tools for investigation of high-frequency and wave dynamic processes, enabling us reliable detection and localization of defects in various parts of machines and structures. This fact has

been confirmed by the computational examples of the cracked rod and beam by respectively similar results obtained using these methods. A very regular character of time histories of the wave propagation processes obtained by means of the proposed approach indicate its high computational accuracy and numerical stability. Moreover, the ranges of time histories in which the simulated responses theoretically should be equal to zero, i.e. the time intervals between passages of successive propagating and reflected waves, in the case of results obtained using the visco-elastic macro-elements, are really almost equal to zero, as it follows from the respective plots. However, in the case of analogous results obtained by means of the spectral finite elements, these theoretically zero-response time-intervals are characterized by the remarkable "numerical dirt" which is particularly visible in Fig. 4c. On the one hand, such computational inaccuracies are not very essential from the practical viewpoint, but when these two methods are mutually compared, one can conclude that the numerical exactness of the proposed approach seems to be even better than that observed in the case of the spectral finite element method. Also slight and not so important (from the viewpoint of the main investigation purpose) differences between these results have been caused by lack of the waveguide excluding unnecessary reflected waves in the discrete-continuous model built by means of the visco-elastic macro-elements. Nevertheless, all these differences vanish when the continuous throw-off macro-element assumed in this paper is applied for the discrete-continuous models of the tested objects. Anyway, the throw-off elements properly applied in the case of both the mutually compared approaches, enable us to simulate the wave responses of unclamped structures too, e.g. not for cantilever rods and cantilever beams only.

According to the above remarks, from the viewpoint of further development of diagnostic wave propagation methods for fault identification in structures, it is worth emphasizing that each theoretical investigation carried out by means of two different methods instead of using only one computational tool is much more reliable, in particular when the corresponding results are very similar to each other. Thus, the straightforward procedures applied in the case of natural visco-elastic continuous macro-elements seem to be very promising for further investigations in this field, when more complex systems and two-dimensional problems will be taken into consideration.

References

1. J.F. DOYLE, *Wave propagation in structures*, Springer-Verlag, New York 1997.

2. M. KRAWCZUK and W. OSTACHOWICZ, *Spectral finite element and genetic algorithm for crack detection in cantilever rod,* Key Engineering Materials, **204–205**, 241–250, 2001.

3. M. Palacz and M. Krawczuk, *Analysis of longitudinal wave propagation in a cracked rod by the spectral element method,* Computer and Structures, **80**, 1809–1816, 2002.

4. W. Ostachowicz, M. Krawczuk and M. Palacz, *Detection of delamination in multi-layer composite beams*, Key Engineering Materials, **245–246**, 483–490, 2003.

5. M. Krawczuk, M. Palacz and W. Ostachowicz, *The dynamic analysis of a cracked Timoshenko beam by the spectral element method*, Journal of Sound and Vibration 264, 1139–1153, 2003.

6. W. Ostachowicz, M. Krawczuk, M. Cartmell and M. Gilchrist, *Wave propagation in delaminated beam*, Computers and Structures 82, 475–483, 2004.

7. M. Krawczuk, M. Palacz and W. Ostachowicz, *Wave propagation in plate structures for crack detection*, Finite Elements in Analysis and Design, **40**, 991–1004, 2004.

8. M. Krawczuk, M. Palacz and Ostachowicz, *Flexural-shear wave propagation in cracked composite beam*, Science and Engieering of Composite Materials, **11**, 1, 55–67, 2004.

9. A. Nag, D. Roy Mahapatra and S. Gopalakrishnan, *Identification of delamination in a composite beam using a damaged spectral element*, Structural Health Monitoring, **1**, 1, 105–126, 2002.

10. T. Szolc, *Dynamic analysis of complex, discrete-continuous mechanical systems* [in Polish], Polish Academy of Sciences – IFTR Reports, 2/2003, *Habilitational dissertation.*

11. R. Bogacz and T. Szolc, *Nonlinear torsional vibration analysis of the drive systems using one-dimensional elastic waves*, Archives of Mechanics, **45**, 1, 65–75, 1993.

12. R. Bogacz, T. Szolc and H. Irretier, *An application of torsional wave analysis to turbogenerator rotor shaft response*, Trans. of the ASME, Journal of Vibration and Acoustics, **114**, 149–153, 1992.

13. T. Szolc, *On the discrete-continuous modeling of rotor systems for the analysis of coupled lateral-torsional vibrations*, International Journal of Rotating Machinery, **6**, 2, 135–149, 2000.

14. T. Szolc, *Medium frequency dynamic investigation of the railway wheelset-track system using a discrete-continuous model*, Archive of Applied Mechanics (Ingenieur Archiv) **68**, 1, 30–45, 1998.

15. T. Szolc, *Simulation of bending-torsional-lateral vibrations of the railway wheelset-track system in the medium frequency range*, Vehicle System Dynamics, **30**, 6, 473–508, 1998.

16. T. Szolc, *Simulation of dynamic interaction between the railway bogie and the track in the medium frequency range*, Multibody System Dynamics, **6**, 99–122, 2001.

17. T. Szolc, T. Bednarek, I. Marczewska, A. Marczewski and W. Sosnowski, *Fatigue analysis of the cracked rotor by means of the one- and three-dimensional dynamical model*, Proc. of the 7th International Conference on Rotor Dynamics, organized by the IFToMM in Vienna, Sept. 2006, Austria 2006, ISBN 3-200-006889-7, Paper No. 241.

18. L. Meirovitch, *Dynamics and Control of Structures*, John Wiley & Sons, New York 1990.

19. A. Pielorz, *Elastic waves in discrete-continuous mechanical systems* [in Polish], Polish Academy of Sciences – IFTR Reports, 21/1992, *Habilitational dissertation* .

20. W. Flügge, *Die Ausbreitung von Biegungswellen in Stäben*, Z. angew. Math. Mech., Bd. 22, **6**, 312–318, 1942.

21. W. Flügge and E.E. Zajac, *Bending impact waves in beams*, Ing.–Archiv, XXVIII, 59–70, Bd. 1959.

22. W. Szcześniak, *Initial conditions in the dynamic investigations of the Timoshenko beam* [in Polish], Scientific Reports of the Warsaw University of Technology – Civil Engineering, **108**, 99–143, Warsaw 1989.